Hindawi
Shock and Vibration
Volume 2018, Article ID 4895862, 8 pages
https://doi.org/10.1155/2018/4895862

Research Article

MEMS Inertial Sensor for Strata Stability Monitoring in Underground Mining: An Experimental Study

Kaizhi Zhang,[1] Songtao Ji,[1,2] Yang Zhang,[3] Jie Zhang,[4] and Ruikai Pan[5]

[1]*School of Mining Engineering, Guizhou Institute of Technology, Guiyang 550003, China*
[2]*School of Earth and Environmental Sciences, The University of Queensland, Brisbane 4067, Australia*
[3]*School of Electrical Engineering and Telecommunications, The University of New South Wales, Sydney 2052, Australia*
[4]*College of Mining and Safety Engineering, Shandong University of Science and Technology, Qingdao 266590, China*
[5]*State Key Laboratory of Coal Mine Disaster Dynamics and Control, Chongqing University, Chongqing 400030, China*

Correspondence should be addressed to Songtao Ji; songtao.ji@uq.edu.au

Received 28 December 2017; Accepted 6 May 2018; Published 4 June 2018

Academic Editor: Caiping Lu

To investigate the fracture and deformation characteristics of the strata in underground mining as well as the effectiveness and sensitivity of the MEMS inertial sensor for strata stability monitoring, a low cost, small size, and easy implementation inertial MEMS sensor module was redeveloped. Sensor modules were installed on roof strata in an underground mining equivalent material simulation experiment. Then, monitoring signal of two modules near the middle and end section of caving strata was processed. The processed signal presents stepped change, and each step consists a vibration stage and a stable stage. Further analysis of each stage, a strategy to estimate the deformation and stability of strata, can be reached: the duration of each vibration stage and complete stage with rising trend indicates that the deformation of strata is growing to the ultimate state. In this study, this method could recognize the destructive deformation of strata at least 1 hour before the strata caving.

1. Introduction

Underground excavation is extensively made for varying purposes such as mining, storage of natural gas and oil, underground powerhouse cavern, and highway and railway tunnels with large sections. As the scale and depth of underground space increase, the risks of roof strata failure become higher due to complex geological environment. In particular, for coal mining, the maximum excavation scale could be up to hundreds and thousands meters in dip and strike direction, respectively. For such scale excavation, it is impossible to maintain the roof strata in stability without deformation; the very core is to monitor the movement characteristics of roof strata, to know when it would be failure, and then to make an accurately warning as early as possible.

In recent decades, numerous monitoring techniques have been conducted to investigate the deformation and stability of the surrounding rock mass in underground excavation. Microseismic (MS) monitoring technique, with remarkable advantages in terms of real time, three-dimensional positioning of mechanical breaking events, has been successfully utilized in underground mining [1–3], powerhouse cavern [4], tunnels [5, 6], and oil and gas extraction [7, 8]. Electrical resistivity tomography [9, 10], acoustic Emission [11], synthetic aperture radar interferometry [12], and many other advanced technologies such as the microwave nondestructive inspection technique [13, 14] were also applied in strength prediction and underground excavation engineering. Those monitoring techniques do make a great contribution for the underground excavation monitoring; however the large scale, complex, and costly monitoring facilities may be the obstacles of applying monitoring system in universal application.

The micro-electro-mechanical systems (MEMS) technology makes it possible to achieve low cost, high precision, small size, wireless, and easy implementation monitoring method to obtain the vibration and motion states of civil structures. For instance, MEMS accelerometers were applied in an exploratory field measurement of ground surface

vibration during an underground blasting [15], to research the characterizations of how the shear zone in a soil mass evolves both spatially and temporally before developing into a full-scale flow landslide in experimental tests [16].

In this paper, a low-cost MEMS inertial sensor, MPU-6050, is conducted to monitor the vibration of roof strata in an underground mining equivalent material simulation experiment. The main objective of this study is to present the effectiveness and sensitivity of the MEMS inertial sensor to strata interfracture and deformation and to develop an early warning strategy for strata deformation and caving.

2. Monitoring System

2.1. Monitoring Method. The strata failure occurs almost instantly, whereas the preparation of failure requires a relatively long-term process, usually accompanied by microstructure crack and macrostructural deformation, which could cause small vibrations and bending deformation. As a matter of fact, not only the strata failure but also the great majority of structure failures would have such processes, which make it possible to characterize these processes by the monitoring data of vibration.

Vibration can be characterized in terms of three parameters: amplitude, velocity, and acceleration. The technology in vibration instrumentation and measurements has advanced significantly over past four decades, particularly in the area of industrial machinery health monitoring. Our study focuses on the vibration caused by rock damage, and a research for the microseismic frequency-spectrum of rock deformation, fracturing, and failure has suggested that the low-frequency components (<25 Hz) of monitoring signals are the key factors for rock damage assessment [17, 18]. The sensitivity of sensors used for measuring these parameters varies with the frequency of the vibration, and the common understanding is to use amplitude sensors to pick up low-frequency signals, velocity sensors in the middle ranges, and accelerometers at higher frequencies (accelerometers mentioned here mainly for the piezoelectric accelerometer). However, to achieve measurement of vibration in one tiny sensor module, we would try to measure the low-frequency vibration by MEMS inertial sensor mpu-6050, which combines a 3-axis gyroscope and a 3-axis accelerometer providing up to ±16 g accelerometer and ±2000°/s gyroscope and output data rate between 4 Hz and 8 kHz [19].

2.2. Monitoring System. To utilize the MEMS sensor in lab and field monitoring, there is a need to develop the signal processing, communication module, and terminal software. The mpu-6050 devices have an onboard Digital Motion Processor™ [19], which processes complex 6-axis Motion Fusion algorithms, but we have conducted a test which reveals that such algorithms may not be suitable in this study for the unstable monitoring data. Several studies [20–25] adopted and developed types of algorithms to obtain better results in terms of acceleration. In this study, we process the signal with the Kalman filter by an onboard STM32 processor (STM8S003); the processed data present the desirable accuracy. Since the sensor has a high sensitivity performance,

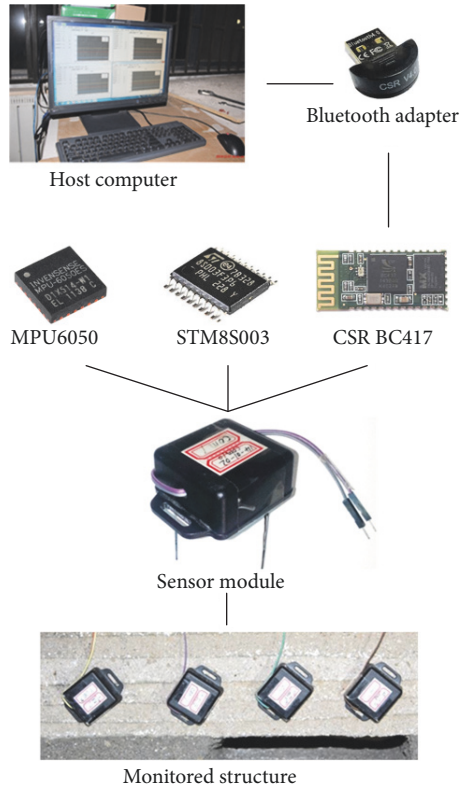

Figure 1: Architecture of monitoring system.

problems can sometimes arise with noise signals induced by the connecting cable. Normally, power supply and signal transmission need 4 single conductor cables; as an improvement, in this case we mount a Bluetooth module (CSR BC417) on the PCB board for wireless communication. Thus, only 2 cables connect with the sensor module which could minimize the measurement error caused by connecting cable vibration. The whole sensor module can then be encapsulated in a 36 × 36 × 15 mm wall-mounting enclosure and total cost of a single sensor module less than 20 dollars. The terminal software for Window OS programmed by C# can display and record the sensor data in real time. The architecture of the monitoring system is shown in Figure 1.

3. Experiment Setup

3.1. Geological Background. The test was conducted in an experimental model based on the "Yushuwan" coal mine located in Yulin city, the region in the northwest part of China. The excavated coal bed 2# was located at the average depth of 180 m undersurface, the thickness of coal seam varies from 1.5~9.4 m, the angle of dip is 0~2°, and mechanical properties of the rocks near coal seam are described in Table 1.

The roof rock strata of coal seam consist of softer rock (mudstone, sandy mudstone) and harder rock (siltstone, gritstone). For the softer rock strata, it would fall following the excavation of coal seam. In contrast, for the harder rock strata, it would not fall until the excavation area meets its strength limit, and if there is no an accurate early warning,

Table 1: Mechanical properties of rocks near coal seam.

Stratum	Thickness h (m)	Parameter				
		Poisson's ratio (ν)	Compressive strength σ_γ (MPa)	Tensile strength σ_t (MPa)	Elastic modulus E (GPa)	Density ρ (kg/m^3)
...	170	-	-	-	-	-
Gritstone	3.3	0.27	65	4.60	5.5	2580
Siltstone	2.6	0.30	72	7.50	9.0	2400
Sandy mudstone	3.1	0.25	26	1.80	3.5	2440
Mudstone	2.2	0.44	19	0.17	1.7	2660
Coal seam	3.6	0.26	14	0.06	1.2	1540
Mudstone	2.5	0.44	19	0.17	1.7	2660
...	-	-	-	-	-	-

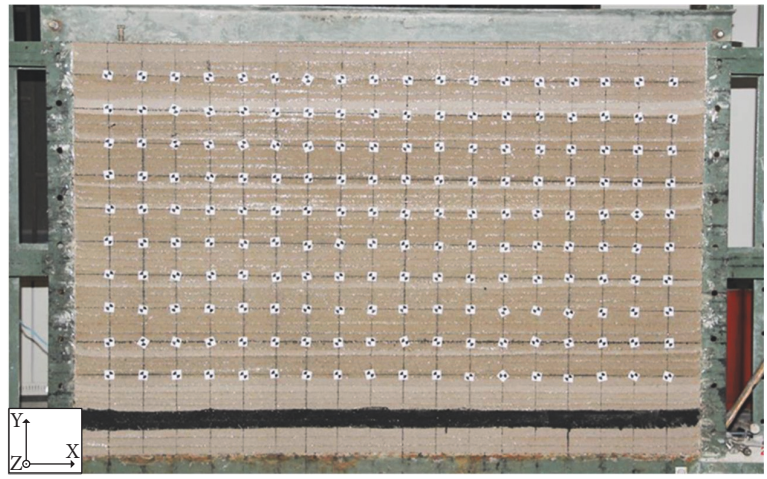

Figure 2: Equivalent material simulation model.

the sudden failure of larger-area rock strata could induce a catastrophic accident. Consequently, the very core is to monitor the movement characteristics of siltstone rock layer, which plays a very important role in the whole roof strata movement.

3.2. Model Building. To investigate the fracture and deformation characteristics of the strata in underground mining, an equivalent material model with scale 1 : 60 size 220 × 180 × 22 cm ($X \times Y \times Z$) is built based on the aforementioned geological background. To simulate the rock strata with various mechanical properties, 4 kinds of materials, sand, calcium carbonate, gypsum, and water, will be mixed in different ratio.

The coal seam, black part shown in Figure 2, will be excavated along the positive direction of x-axis from x = 15 cm. In order to cover key positions of fracture and deformation as much as possible, 4 sensor modules, numbers S1–S4, are installed on the siltstone stratum at section of x = 17, 27, 37, and 47 cm, as shown in Figure 3. The sensor module can be set to the initial state; therefore the installation errors would not affect the accuracy of monitoring.

3.3. Excavation. With the increase of the excavation area, the overlying mudstone and sandy mudstone stratum cave into small blocks (see Figure 4(a)), and the siltstone, gritstone, and upper strata structure cave suddenly when the excavation distance reaches 50 cm (see Figure 4(b)). From Figure 4(b) we learn that 3 sensor modules S2–S4 are at the caving part of siltstone stratum, S1 is at the uncaving suspended part, and S2 is the nearest one to the end section with most obvious inclination angle change. Digging further into the strata fractures layout, we can also find cracks mainly located at middle section of strata, and S3 is the nearest one to the middle section.

4. Monitoring Results Analysis

In terms of acceleration, theory of beam on elastic foundation has been revealed: for roof strata in underground mining, the middle section and end section are the key parts, withstanding a maximum shear force and bending moment, and could present more precursory vibration signals as well [26–29]. Regarding the relative location of sensors to the fractured strata, S1 is located at the stable cantilever strata and

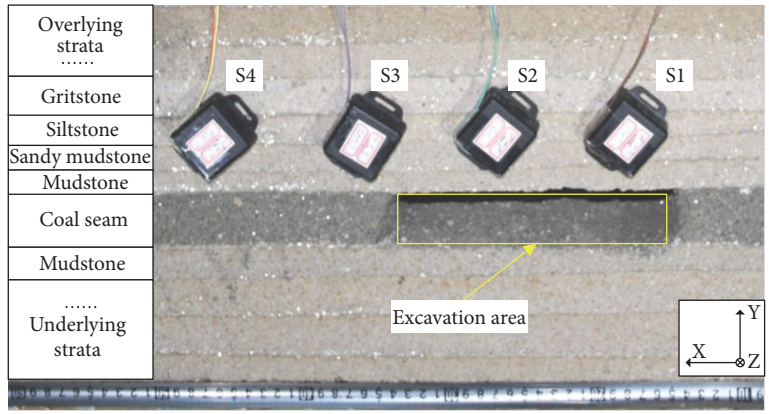

Figure 3: Sensor modules layout.

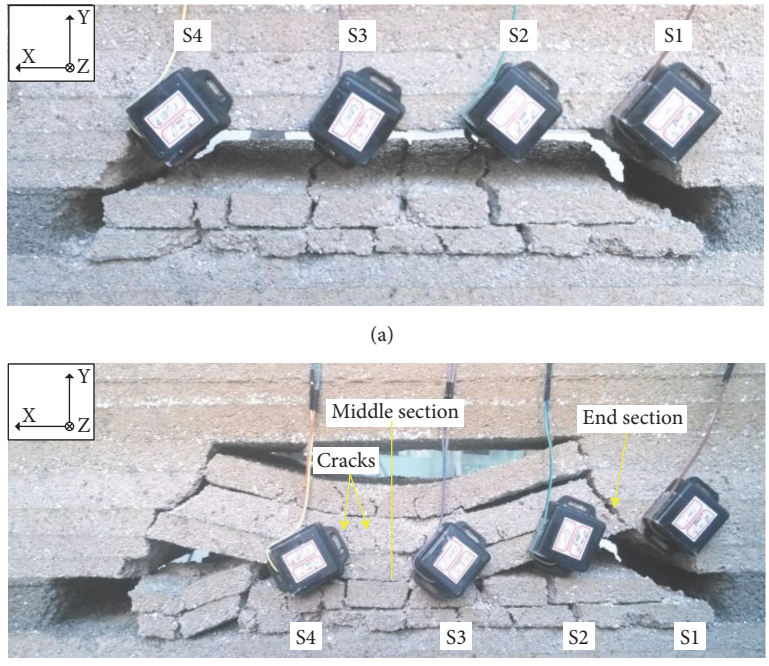

Figure 4: Roof strata caving with excavations. (a) Excavation distance = 40 cm. (b) Excavation distance = 50 cm.

S2, S3, and S4 are located at failure strata, among which S2 and S3 are located at the right side of middle section and S4 is located at the other side. This means that sensors can be divided into 3 groups, with various movement characteristics, in accordance with the different position of strata structure. Considering that S2 and S3 are the nearest sensors to the middle section and end section, respectively, in addition, both S2 and S3 located at the same structure area that can be compared to each other. Hence, the monitoring data of S2 and S3 will be further analyzed.

4.1. Signal Processing. In order to present the data more directly and clearly, we set 6000 seconds before fracture as time 0 and set the acceleration data at the time 0 to 0 as well. Figures 5(a) and 5(b) are the original acceleration signal data of S2 and S3 in x-axis 100 minutes before strata fracture, respectively.

Figure 5(a) shows the acceleration signals of S2 fluctuate around 0 (±0.002 g) and then witnessed a rapid rise since 5800 s caused by strata rotational deformation near the end section. Figure 5(b) shows that S3 signals keep a state of fluctuation without any marked changes until 6000 s that tally with a middle section movement characteristic of a beam structure. The dramatic growth of S2 indicates that the macroscopic movement of different strata parts before 5800 s is the same in general. However, as a preparation process more features need to be extracted and analyzed at the microlevel; therefore, the signal should be postprocessed.

As illustrated in Figure 6(a), it is almost impossible to read effective features from the original signal as undesirable

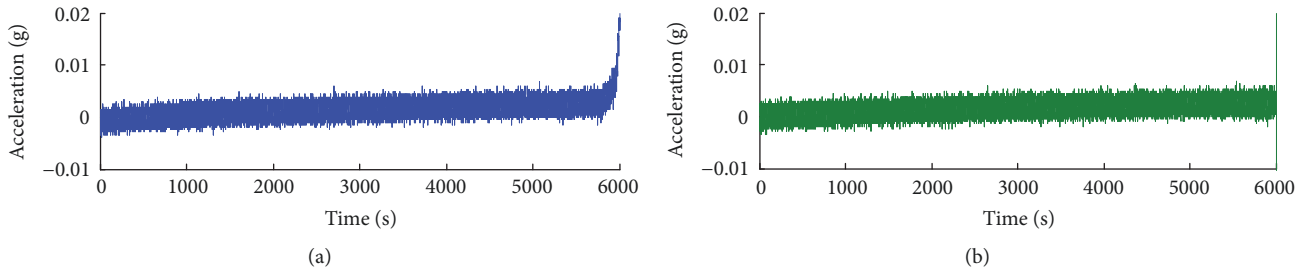

Figure 5: Original acceleration signal. (a) Sensor module S2. (b) Sensor module S3.

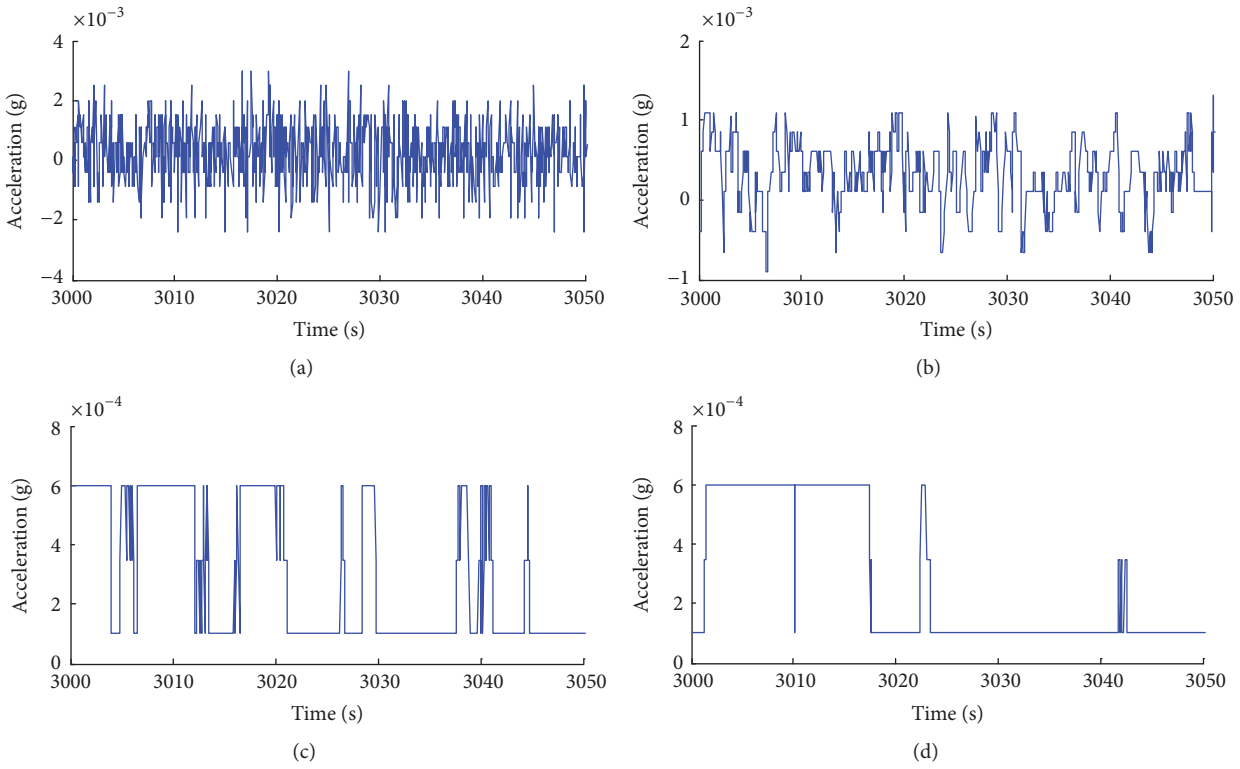

Figure 6: Acceleration signal of S2 in 3000–3050 s. (a) Original signal. (b) Processed by median filter with $n = 10$. (c) Processed by median filter with $n = 100$. (d) Processed by median filter with $n = 250$.

noises. To further investigate the signal features, signals will be processed by a median filter to remove the noise and to keep important features as much as possible [30–32]. Figures 6(b)–6(d) shows the signal processed by the median filter with different n (order of the one-dimensional median filter). Signal shown in Figure 6(b) has a similar but better result (±0.001 g) than Figure 6(a), the original one; however it is still hard to tell the signal features. Figures 6(c) and 6(d) further improve the signal performance to a desirable level (±0.00025 g); in particular, Figure 6(d) filtrates most of the noise, meanwhile keeping main characteristics of the original signal.

4.2. Signal Analysis. According to the filtering performance, the acceleration signals of S2 and S3 will be processed with the same setting in Figure 6(d) and the processed data as shown in Figure 7.

This figure describes that there are 6 discontinuous vibration stages, from I to VI, within 6000 s. The periodic change of signal means that both the middle and end sections of strata will go through 6 periods of internal structural fracture, and after a period of fracture the strata will be relatively stable without new fractures for a period of time and then to the next period of fracture, and so on until strata caving. As the component of the gravity acceleration in x-axis is rising, so there is an acceleration difference, 5×10^{-4} g, between 2 adjacent stages. Thus, the signal with stage change and rising trend is caused not only by the internal structural fractures of strata, but also by the deformation.

For the convenience of analysis, we define the concept of "vibration stage" as each signal vibration part from the start time to the end time; for more details see Table 2; we define the concept of "complete stage" as the part from the start of a vibration stage to the start of next vibration stage; for instance,

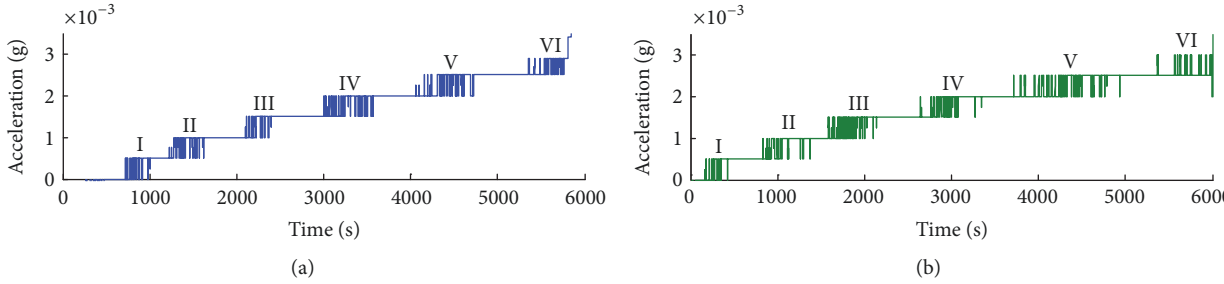

Figure 7: Acceleration signal processed by median filter with $n = 250$. (a) Sensor module S2. (b) Sensor module S3.

Table 2: Start and end time of vibration stages (s).

	I	II	III	IV	V	VI
S1	725–1002	1224–1619	2105–2397	3001–3567	4055–4727	5359–caving
S2	127–430	830–1371	1587–2138	2637–3347	3709–4935	5369–caving

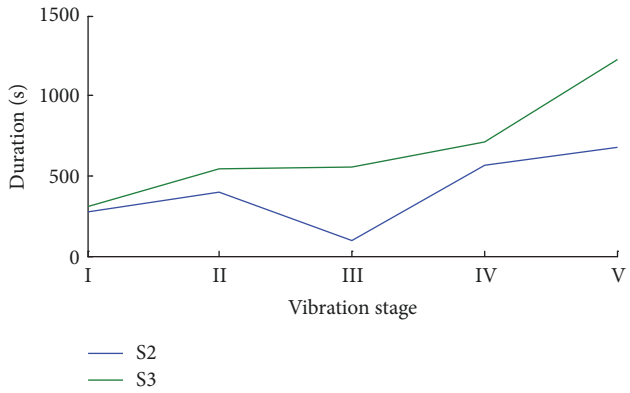

Figure 8: Duration of vibration stage.

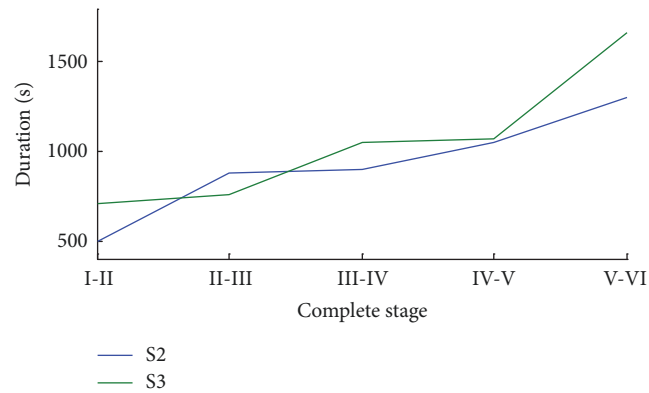

Figure 9: Duration of complete stage.

complete stage S2 (I-II) is the time period from 725 s to 1224 s.

The duration of each vibration stage, except stage VI caused by strata caving, can be calculated by the data of Table 2, as shown in Figure 8. The line graph illustrates that the duration of S2 and S3 saw an upward trend in general, which means that internal structural fractures increased gradually whilst the strata got closer to caving. Meanwhile, the S3 green line keeps in above of the S2 blue line; namely, the durations of S3 last longer than S2 at each stage, which indicates that the fractures at middle section of strata last longer than that at end section. In fact, this may be explained by Figure 4(b); we can find more observed unpenetrating fractures located at the middle section and only one penetrating fracture at the end section, which is the end section itself.

Furthermore, in terms of the complete stage, the duration of each complete stage can be achieved from Table 2, shown in Figure 9. And the lines show a steady climb, without exception, to the highest point at the last vibration stage. This change pattern could offer a new way to make an early warning of strata instability. In this study, this trend of change can be observed at least 1 hour before strata caving.

5. Conclusions

In this study, low-cost MEMS inertial sensor modules are adopted to investigate the fracture and deformation characteristics of the overlying strata in an underground mining equivalent material simulation experiment. The monitoring data of two sensor modules, near to the middle section and end section of suspended strata, are processed by median filter. Processed data shows that the median filter is an effective signal processing method for the denoising of acceleration data. Furthermore, comparison and statistical analysis are conducted to investigate the movement characteristics of strata prior to the first weighting, and then the following conclusions can be drawn:

(1) The effectiveness and sensitivity of the low-cost MEMS inertial sensor, less than 20 dollars, to strata interfracture and deformation, are tested and proofed.

(2) The strata deformation presents a characteristic of step change, rather than continuous change; each step consists of two parts: a vibration stage and a stable stage.

(3) The duration of each single period with rising trend indicates that the deformation of strata is growing to the ultimate state, which could be as a criterion for early warning and recognizing the destructive deformation of strata.

The experimental test results demonstrate the validity of the MEMS inertial sensor; theoretically, for an underground excavation only 2 sensor modules are required. This approach may hopefully serve as a new low-cost monitoring method applied in related research areas and engineering practice.

Conflicts of Interest

The authors declare no conflicts of interest.

Acknowledgments

This study is financially supported by Major Innovation Group Project of Guizhou Education Department (KY [2016]042), National Natural Science Foundation of China (no. 51564004), and the China Scholarship Council.

References

[1] L. J. Dong and X. B. Li, "A microseismic/acoustic emission source location method using arrival times of PS waves for unknown velocity system," *International Journal of Distributed Sensor Networks*, vol. 2013, Article ID 307489, 8 pages, 2013.

[2] L. Dong, D. Sun, X. Li, and K. Du, "Theoretical and Experimental Studies of Localization Methodology for AE and Microseismic Sources Without Pre-Measured Wave Velocity in Mines," *IEEE Access*, vol. 5, pp. 16818–16828, 2017.

[3] E. C. Westman, R. J. Molka, and W. J. Conrad, "Ground control monitoring of retreat room–and–pillar mine in Central Appalachia," *International Journal of Mining Science and Technology*, vol. 27, no. 1, pp. 65–69, 2017.

[4] F. Dai, B. Li, N. Xu, and Y. Zhu, "Microseismic early warning of surrounding rock mass deformation in the underground powerhouse of the Houziyan hydropower station, China," *Tunnelling and Underground Space Technology*, vol. 62, pp. 64–74, 2017.

[5] G.-L. Feng, X.-T. Feng, B.-R. Chen, Y.-X. Xiao, and Q. Jiang, "Sectional velocity model for microseismic source location in tunnels," *Tunnelling and Underground Space Technology*, vol. 45, pp. 73–83, 2015.

[6] C. Liu, S. Li, C. Cheng, and X. Cheng, "Identification methods for anomalous stress region in coal roadways based on microseismic information and numerical simulation," *International Journal of Mining Science and Technology*, vol. 27, no. 3, pp. 525–530, 2017.

[7] M. Haddad, J. Du, and S. Vidal-Gilbert, "Integration of dynamic Microseismic data with a true 3D modeling of hydraulic fracture propagation in Vaca Muerta Shale," in *Proceedings of the SPE Hydraulic Fracturing Technology Conference, HFTC 2016*, USA, February 2016.

[8] M. J. Mayerhofer, E. P. Lolon, J. E. Youngblood, and J. R. Heinze, "Integration of microseismic fracture mapping results with numerical fracture network production modeling in the Barnett shale," in *Proceedings of the SPE Annual Technical Conference and Exhibition (ATCE '06)*, pp. 976–983, San Antonio, Tex, USA, September 2006.

[9] N. Lesparre, D. Gibert, F. Nicollin, C. Nussbaum, and A. Adler, "Monitoring the excavation damaged zone by three-dimensional reconstruction of electrical resistivity," *Geophysical Journal International*, vol. 195, no. 2, pp. 972–984, 2013.

[10] H. Kiflu, S. Kruse, M. H. Loke, P. B. Wilkinson, and D. Harro, "Improving resistivity survey resolution at sites with limited spatial extent using buried electrode arrays," *Journal of Applied Geophysics*, vol. 135, pp. 338–355, 2016.

[11] M. Cai, H. Morioka, P. K. Kaiser et al., "Back-analysis of rock mass strength parameters using AE monitoring data," *International Journal of Rock Mechanics and Mining Sciences*, vol. 44, no. 4, pp. 538–549, 2007.

[12] U. Wegmuller, T. Strozzi, C. Werner, A. Wiesmann, N. Benecke, and V. Spreckels, "Monitoring of mining-induced surface deformation in the Ruhrgebiet (Germany) with SAR interferometry," in *Proceedings of the 2000 Internaitonal Geoscience and Remote Sensing Symposium (IGARSS 2000)*, pp. 2771–2773, July 2000.

[13] K. L. Chung, C. Zhang, Y. Li, L. Sun, and M. Ghannam, "Microwave non-destructive inspection and prediction of modulus of rupture and modulus of elasticity of engineered cementitious composites (ECCs) using dual-frequency correlation," *Sensors*, vol. 17, no. 12, article no. 2831, 2017.

[14] K. L. Chung, J. Luo, L. Yuan, C. Zhang, and C. Qu, "Strength correlation and prediction of engineered cementitious composites with microwave properties," *Applied Sciences (Switzerland)*, vol. 7, no. 1, article no. 35, 2017.

[15] G. L. Ooi and Y. H. Wang, "Applying MEMS accelerometers to measure ground vibration and characterize landslide initiation features in laboratory flume test," in *Proceedings of the 2014 Congress on Geo-Characterization and Modeling for Sustainability, Geo-Congress 2014*, pp. 2019–2028, USA, February 2014.

[16] G. L. Ooi, P. S. Tan, M. Lin, K. Wang, Q. Zhang, and Y. Wang, "Near real-time landslide monitoring with the smart soil particles," *Japanese Geotechnical Society Special Publication*, vol. 2, no. 28, pp. 1031–1034, 2016.

[17] C.-P. Lu, L.-M. Dou, N. Zhang et al., "Microseismic frequency-spectrum evolutionary rule of rockburst triggered by roof fall," *International Journal of Rock Mechanics and Mining Sciences*, vol. 64, pp. 6–16, 2013.

[18] C.-P. Lu, G.-J. Liu, Y. Liu, N. Zhang, J.-H. Xue, and L. Zhang, "Microseismic multi-parameter characteristics of rockburst hazard induced by hard roof fall and high stress concentration," *International Journal of Rock Mechanics and Mining Sciences*, vol. 76, pp. 18–32, 2015.

[19] InvenSense MPU-6050 Data Sheet Revision 4.2, 2015, https://www.invensense.com/wp-content/uploads/2015/02/MPU-6000-Datasheet1.pdf.

[20] A. Benini, A. Mancini, A. Marinelli, and S. Longhi, "A Biased Extended Kalman Filter for indoor localization of a mobile agent using low-cost IMU and UWB wireless sensor network," in *Proceedings of the 10th IFAC Symposium on Robot Control, SYROCO 2012*, pp. 735–740, hrv, September 2012.

[21] M. Ruizenaar, E. van der Hall, and M. Weiss, "Gyro bias estimation using a dual instrument configuration," in *Proceedings of the 2nd CEAS Specialist Conference on Guidance*, Navigation & Control, 2013.

[22] H. Hyyti and A. Visala, "A DCM Based Attitude Estimation Algorithm for Low-Cost MEMS IMUs," *International Journal of Navigation and Observation*, vol. 2015, Article ID 503814, 2015.

[23] M. T. Leccadito, T. Bakker, R. Niu, and R. H. Klenke, "A kalman filter based attitude heading reference system using a low cost inertial measurement unit," in *Proceedings of the AIAA Guidance, Navigation, and Control Conference, 2015*, USA, January 2015.

[24] L. Kang, L. Ye, K. Song, and Y. Zhou, "Attitude heading reference system using MEMS inertial sensors with dual-axis rotation," *Sensors*, vol. 14, no. 10, pp. 18075–18095, 2014.

[25] R. Munguia and A. Grau, "An attitude and heading reference system (AHRS) based in a dual filter," in *Proceedings of the Proceeding pf the IEEE 16th Conference on Emerging Technologies & Factory Automation (ETFA '11)*, pp. 1–8, Toulouse, France, September 2011.

[26] Y. Pan, S. Gu, and Y. Qi, "Analytic solution of tight roof's bending moment, deflection and shear force under advanced super charger load and supporting resistance before first weighting," *Chinese Journal of Rock Mechanics and Engineering*, vol. 32, pp. 1545–1553, 2013.

[27] S. Xie, H. Pan, D. Chen, M. Gao, S. He, and B. Song, "The structure and activity laws of interlayer equivalent basic roof in multi-seam mining," *Journal of China University of Mining and Technology*, vol. 46, no. 6, pp. 1218–1225, 2017.

[28] S. Ji, C. Zhang, and K. Zhang, "An analytical approach to determine the span and fracture positions of roof strata prior to rock burst," in *Mechanics of Structures and Materials XXIV: Proceedings of the 24th Australian Conference on the Mechanics of Structures and Materials*, pp. 345–350, Perth, Australia, 2016.

[29] M. He, S. Chen, Z. Guo, J. Yang, and Y. Gao, "Control of surrounding rock structure for gob-side entry retaining by cutting roof to release pressure and its engineering application," *Journal of China University of Mining and Technology*, vol. 46, no. 5, pp. 959–969, 2017.

[30] M. Fraser, A. Elgamal, X. He, and J. P. Conte, "Sensor network for structural health monitoring of a highway bridge," *Journal of Computing in Civil Engineering*, vol. 24, no. 1, pp. 11–24, 2010.

[31] V. N. Guruprakash and R. Ganguli, "Optimally weighted recursive median filters for denoising vibration signals used in health monitoring of rotating systems," *ISSS Journal of Micro and Smart Systems*, vol. 6, no. 1, pp. 47–55, 2017.

[32] N. Roy and R. Ganguli, "Filter design using radial basis function neural network and genetic algorithm for improved operational health monitoring," *Applied Soft Computing*, vol. 6, no. 2, pp. 154–169, 2006.